frontiers | Frontiers in Materials

TYPE Original Research
PUBLISHED 01 December 2022
DOI 10.3389/fmats.2022.1084906



OPEN ACCESS

EDITED BY
Bing Bai,
Beijing Jiaotong University, China

REVIEWED BY
Yong Yuan,
China University of Mining and Technology, China
Yu Wang,
University of Science and Technology Beijing, China

*CORRESPONDENCE
Zhangjun Dai,
zjdai@whrsm.ac.cn

SPECIALTY SECTION
This article was submitted to Structural Materials,
a section of the journal
Frontiers in Materials

RECEIVED 31 October 2022
ACCEPTED 21 November 2022
PUBLISHED 01 December 2022

CITATION
Dai Z, Wang Y, Zhou Z, Li J, Yu F and Chen S (2022), Analysis of the deterioration process of the dolomite with the interlayer in different directions during wetting.
*Front. Mater.* 9:1084906.
doi: 10.3389/fmats.2022.1084906



# Analysis of the deterioration process of the dolomite with the interlayer in different directions during wetting

Zhangjun Dai[1]*, Yinhui Wang[1,2], Zhe Zhou[1,2], Jian Li[1], Fei Yu[1] and Shanxiong Chen[1]

[1]State Key Laboratory of Geomechanics and Geotechnical Engineering, Institute of Rock and Soil Mechanics, Chinese Academy of Sciences, Wuhan, China, [2]University of Chinese Academy of Sciences, Beijing, China

Taking the dolomite with anhydrite interlayer at the bottom of Huangcaoshan Tunnel in Shanghai-Wuhan-Chengdu high-speed railway as the research object, the wetting deterioration and uniaxial compression tests were performed to study the influence of different interlayer orientations on the hygroscopic deterioration characteristics of rock and to analyze the process of rock deterioration. The wetting cracking and deformation characteristics of dolomite with interlayer in different directions were analyzed respectively from the time effect of rock micro-expansion and the change of ultrasonic longitudinal wave velocity, and the uniaxial compression evolution process of samples with different moisture absorption conditions and interlayer directions was analyzed respectively from the aspects of crack volume strain and energy dissipation. The results show that the direction of interlayer had a significant effect on the wetting and deterioration of the rock. The sample with vertical interlayer cracked obviously during wetting, resulting in volume expansion along the axial and radial directions of the sample; However, the sample with horizontal interlayer had almost only axial volume expansion, and the expansion rate was small. After the rock was wet and deteriorated, the propagation velocity of ultrasonic longitudinal wave in the rock decreased, and the decrease amplitude in the sample with vertical interlayer was greater than that in the sample with horizontal interlayer. After rock wetting, its uniaxial compressive strength, crack initiation level, expansion level, and the threshold value of elastic strain energy density for failure decreased, while the radial peak strain, the energy conversion rate of dissipation increased, and the plastic characteristics of the sample were enhanced, and the sample with vertical interlayer changed significantly compared with the sample with horizontal interlayer.

KEYWORDS

**deterioration process, dolomite, anhydrite, interlayer, wetting, uniaxial compression**

# 1 Introduction

Water rock interaction exists widely in various practical geotechnical engineering. Under the action of water, the rock will often be softened, cracked, expanded, disintegrated and other deterioration phenomena (Zhao et al., 2021; Zhou K. et al., 2022; Feng et al., 2022; Li et al., 2022), and this deterioration of rock in water has a great impact on the safety of various engineering construction (Bai et al., 2021; Du et al., 2022; Fu et al., 2022). Therefore, the research on the law of rock wetting deterioration has always been the focus of researchers (Jiang et al., 2015; Hua et al., 2019).

In terms of the cracking, disintegration and expansion effect of rocks under the action of water and rock. Zeng et al. (2019) took the completely disintegrated carbonaceous mudstone as the research object, and used the image processing technique to analyze the crack evolution process and geometric characteristics of the sample under the action of dry-wet cycle. Chai et al. (2015) based on the comparative test of the slaking resistance of mudstone in coal measures in different diagenetic stages, used XRD (X-ray Diffraction) and mercury intrusion tests to find that the difference in the slaking resistance of mudstone was mainly related to the mineral composition, rock pore and crack structure. Yang (2017), Diao et al. (2017) studied the hygroscopic expansion characteristics and water migration laws of mudstone under different temperature and humidity conditions. He et al. (2019) carried out indoor expansion characteristics tests on red-bed soft rocks of different lithology in a tunnel area, and found that the logarithm of expansion force was linear with expansion strain, the expansion force was positively correlated with dry unit weight and water absorption, and negatively correlated with initial moisture content. Ma (2015) studied the deformation law, development process, development stage and micro expansion mechanism of the micro expansion deformation of low clay mineral mudstone.

In terms of softening of the mechanical properties of rocks under the action of water and rock, Zhou et al. (2005) conducted mechanical tests on different types of rocks such as sandstone, mudstone and carbonaceous mudstone with different immersion times, and found that their compressive strength, tensile strength and shear strength decreased exponentially with the saturation time. Cai et al. (2021) conducted direct shear tests on phyllite under different immersion conditions and found that the cohesion was most affected by immersion conditions, the peak stress was second, and the internal friction angle was the smallest. Jiang et al. (2022) established the damage constitutive model of sandstone under the water rock interaction through the experimental analysis, combined with the deduction of statistical strength theory and damage mechanics. Uniaxial compression characteristics, as one of the indispensable indexes to measure the basic physical and mechanical properties of rocks, are widely used in various engineering practices and scientific research work because of its relatively simple and clear test principles and easily realized test equipment. He et al. (2022) carried out uniaxial compression test on sandstone, and found that with the increase of moisture content, the nonlinear characteristics of the rock stress-strain curve at the initial stage and the drop phenomenon after the strength peak became more obvious, and the sample changed from splitting failure to shear failure. Song et al. (2021) established a sandstone deterioration model under dry wet cyclic loading through uniaxial compression test and acoustic emission testing technology. Zhang et al. (2020) compared the difference of stress threshold under different calculation methods based on the uniaxial compression test of siliceous siltstone, and provided an optimization method for obtaining the stress threshold. Zhang et al. (2021) analyzed the influence of the crack dip angle on the crack initiation stress, peak strength, stress-strain curve characteristics and failure mode of rock during uniaxial compression. Hou et al. (2019) explored the anisotropy law in the process of rock energy conversion through energy analysis of the uniaxial compression process of layered marble. Tang et al. (2022) studied the influence of loading rate on energy evolution characteristics during uniaxial compression of rocks.

Therefore, researchers have made a lot of achievements in the study of rock wetting deterioration effect. However, the previous studies mostly focused on the deterioration effect of relatively homogeneous soft rock, while the research on the wetting deterioration effect of hard rock containing expansive materials in non-expansive rock, especially on the change of rock uniaxial compression characteristics before and after deterioration, was less. For this reason, this study selected dolomite with anhydrite interlayer at the tunnel bottom in the abnormal deformation section of high-speed railway as the research object, conducted wetting deterioration test on it, obtained the change characteristics of free expansion rate with time, and quantitatively evaluated its deterioration based on the measured changes of acoustic velocity before and after deterioration. Finally, based on the uniaxial compression test, the uniaxial compression process was analyzed from the perspective of crack volume strain and energy dissipation, and the effects of different interlayer directions and wetting conditions on the compression process and mechanical characteristics were compared. This study revealed the mechanism of moisture absorption expansion and deterioration of interlayered dolomite, and provided a scientific basis for the analysis of abnormal deformation of subgrade and track, especially uplift deformation of high-speed railway and other projects. It provided important reference for railway engineering construction and geological disaster prevention.

# 2 Materials

## 2.1 Engineering geological characteristics

The sampling site was located in Huangcaoshan Tunnel, Changshou County, Chongqing, China. This tunnel was a high-

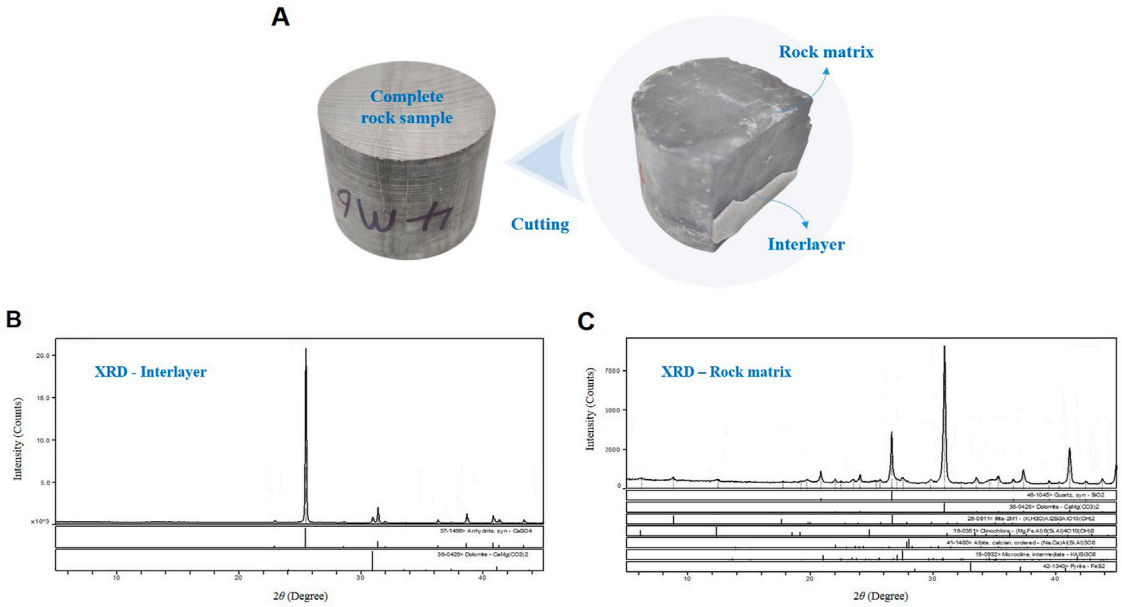


FIGURE 1
XRD pattern for the dolomite with the interlayer **(A)** Schematic diagram of rock matrix and interlayer **(B)** XRD pattern for interlayer **(C)** XRD pattern for rock matrix.

speed railway tunnel, and the stratum it passed through was located at the top of a box anticline. The rock stratum at the tunnel bottom was Leikoupo Formation of Middle Triassic ($T_2l$), mainly composed of gray and light gray dolomite and limestone, medium-thick layered, with good water permeability. There were thin layers of gypsum and anhydrite in the rock stratum. The rock samples used in this study were mainly dolomite. The rock was relatively complete with developed cracks. Some rock samples had no complete structure and were scattered. The average density of rock samples was 2.83 g/cm$^3$, the moisture content ranges from 0.03% to 0.29%, and the average moisture content was 0.20%.

## 2.2 Mineral composition

The rock sample contains interlayers. Samples were taken from the rock matrix and interlayers respectively. After rolling, it should pass 0.05 mm sieve, and then it was dried for preparation. The mineral composition was analyzed by X-ray diffraction. The analysis results were shown in Figure 1. Anhydrite occurred in dolomite in the form of thin interlayer, visible to the naked eye, with the thickness between 0.1 and 2.0 mm, and most of them were less than 0.5 mm. The rock was mainly composed of dolomite, containing a certain amount of clay minerals (illite, chlorite, *etc.*) and siliceous (quartz) cements, and anhydrite, an expansive mineral, also accounted for a certain proportion in the rock. Among them, in the interlayer, anhydrite accounted for 93.1% and dolomite accounted for 6.9%. The rock matrix consisted of 73.9% dolomite, 13.8% quartz, 8.0% clay minerals, and a small amount of feldspar and pyrite.

## 2.3 Microstructure

The microstructure of different parts of the sample was analyzed by scanning electron microscope. Figure 2 shows the rock SEM (Scanning Electron Microscope) microstructure. It showed that dolomite, anhydrite, illite and other mineral particles could be seen in the rock. Most dolomite crystals were in the form of semi idiomorphic to idiomorphic inlaid contact, with flat boundaries, and the crystals were mostly connected by crystal planes (Figure 2A). The anhydrite crystal structure was compact fiber collection, plate or sheet stacking, and its fibrous crystal features were obvious. The crystals were closely arranged, orderly, multi-layer overlapping, three-dimensional, and the crystal surface was smooth and shiny, with occasional bumps and depressions (Figure 2B). The results also showed significant flocculent clay mineral distribution, some of which had obvious microcracks. The clay particles were curved and curly, and most of them were in the form of face to face overlapping and

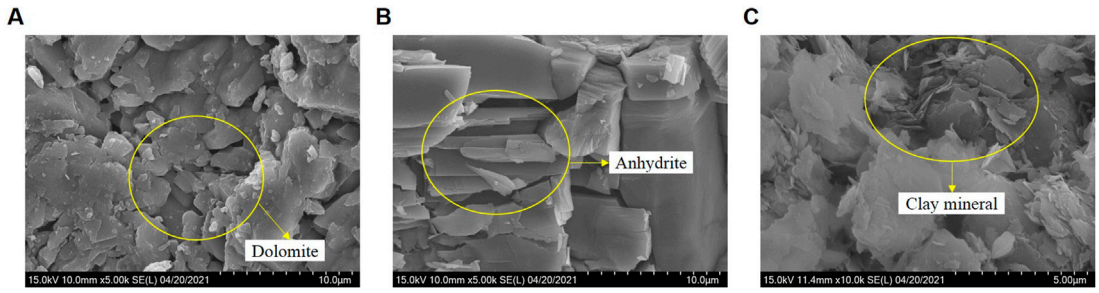


FIGURE 2
SEM results **(A)** Dolomite **(B)** Anhydrite **(C)** Clay mineral.

edge to face overlapping, thus forming a relatively dense form (Figure 2C).

From the XRD and SEM test results, it could be seen that the rock had the potential of expansion and wetting deterioration. It provided the material and structural basis for the interlayer effect and crack expansion effect of rock.

## 3 Deterioration characteristics of rocks in different interlayer directions after wetting

The free expansion rate is the ratio of the increment of rock expansion to the initial size of the sample under no load conditions. The obtained rock was polished and made into the sample, and then put it into a self-developed dilatometer for three-way expansion rate test. After water injection, observed the three-dimensional deformation of the sample, and monitored the rock cracking characteristics and expansion time history change law.

Many researchers have found that there is a positive correlation between the longitudinal wave velocity and the compactness of the rock's internal structure (Anderson et al., 1974; King et al., 1995; Jia et al., 2019). The denser and more uniform the structure, the higher the wave velocity value. On the contrary, if the sample is looser and the internal voids are more, the measured wave velocity will be lower. Therefore, in this study, the corresponding samples were taken for rock acoustic velocity test to explore the change of longitudinal wave velocity of rock under the initial conditions of samples and after immersion and air drying.

### 3.1 Sample preparation

The test samples were taken from the tunnel bottom in the abnormal deformation section of the high-speed railway Huangcaoshan Tunnel. The samples were taken from the rock stratum by means of drilling and sampling, and the core drilling and cutting processing were carried out in the laboratory. In order to reduce the dispersion of the samples, the original rocks of the test samples were taken from the same location at the tunnel bottom. Limited to the on-site drilling conditions and considering as much as possible the interlayers of the samples, the rock was processed into cylinder samples with the diameter of 50 mm and the height of 40 mm, and their two ends and sides were carefully polished to make the unevenness of both ends less than 0.05 mm.

### 3.2 Wetting deterioration test

In order to facilitate the subsequent test and realize the uniaxial compression of the sample along the interlayer direction after wetting and deterioration, a group of vertical interlayer samples (JZ-1, JZ-2, JZ-3) was selected for the free expansion rate test, and another group of horizontal interlayer samples (JH-1, JH-2, JH-3) was taken as the control group. The schematic diagram of core drilling sampling and finished samples are shown in Figure 3. The acoustic longitudinal wave velocity of rock was tested under the initial conditions and after the natural conditions were dried until the sample quality no longer changes after immersion, and the acoustic wave velocity changes before and after rock wetting and deterioration were analyzed.

The self-developed three-way expansion rate instrument was used to conduct the three-way free expansion rate test of rock, as shown in Figure 4. Holes were reserved in the center of the plexiglass on four sides, and dial indicators were installed to monitor the radial deformation of the sample. A dial indicator was equipped on the top of the instrument to monitor the axial deformation of the sample.

Rock acoustic velocity test adopted ultrasonic pulse penetration method to conduct longitudinal wave test on samples. The test instrument was RSM-SY6 intelligent acoustic detector produced by Institute of Rock and Soil

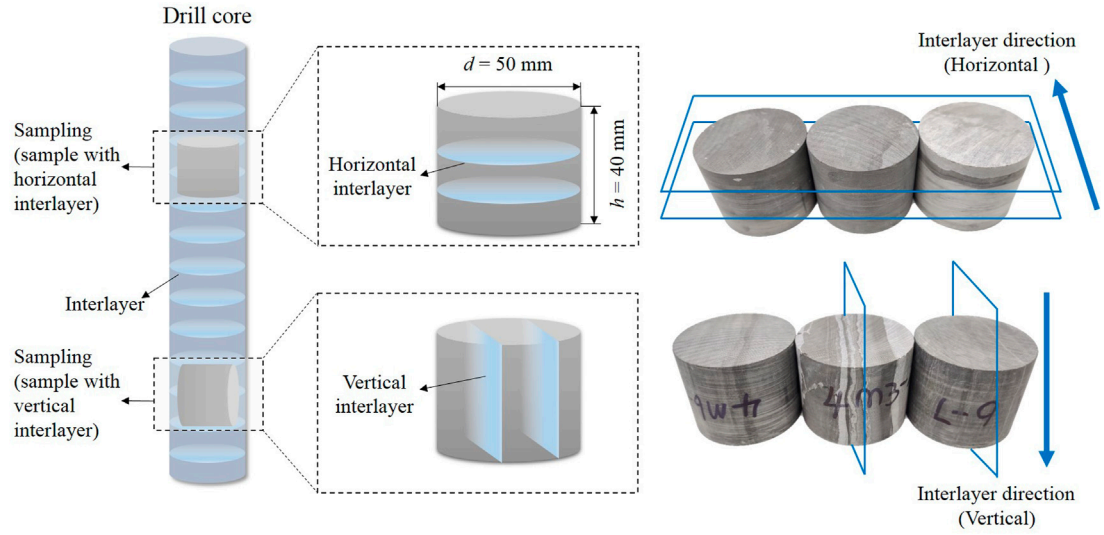


FIGURE 3
Sampling diagram and dolomite sample with interlayer in different directions.

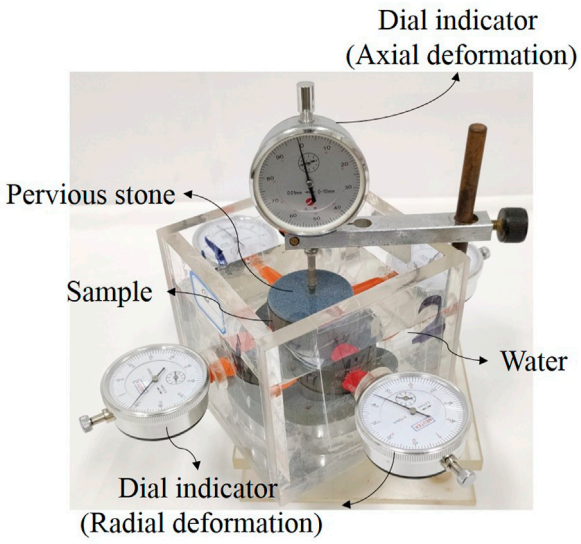


FIGURE 4
Test device for three-way expansion rate of rock.

Mechanics, Chinese Academy of Sciences. The low pass frequency of longitudinal wave transducer was 60 kHz, the high pass frequency was 0.1 kHz, and the sampling interval was 0.1 μs. During the test, ultrasonic flaw detection couplant was used to couple the longitudinal wave transducer with the sample, and a certain pressure was applied to make the transducer closely fit with the end face of the sample, and longitudinal wave velocity was tested one by one.

## 3.3 Analysis of deterioration characteristics of rock after wetting

The final axial and average radial expansion rates of each sample are shown in Table 1. Each sample of the vertical interlayer had obviously cracked after immersion, as shown in Figure 5. The main cracks developed along the direction of the interlayer, accompanied by a small number of secondary cracks with a certain angle to the vertical direction. After the test, the sample was looser than the original sample, which was also consistent with the results of longitudinal wave velocity test of rock. Although the horizontal interlayer sample had axial and radial expansion, the expansion amount was obviously smaller than that of the vertical interlayer sample, and the sample had no obvious cracking.

Figure 6 shows the change curves of the axial and average radial expansion rates with time for the typical JZ-3 sample with vertical interlayer and JH-2 sample with horizontal interlayer respectively. The sample with vertical interlayer reached stability after 58 h, and the whole process of immersion expansion and deformation of the sample in axial and radial directions could be divided into four stages, starting stage, rapid growth stage, decelerating growth stage and gradually stabilizing stage. The final average radial expansion rate of the sample was 0.728%, the axial expansion rate was 0.470%, and the average radial expansion rate was 54.9% greater than the axial expansion rate. However, the sample with horizontal interlayer reached stability after 86 h, and its axial and radial expansion rate curves were all in a stepwise rising shape, that was, after the initial rapid growth stage, the sample entered a deceleration or gradually stable stage, but after a period of time, it would continue to enter

TABLE 1 Test results of expansion rate and longitudinal wave velocity.

| Sample no. | Density of undisturbed sample (kg/m$^3$) | Axial expansion rate (%) | Average radial expansion rate (%) | Longitudinal wave velocity (m/s) | | Decrease rate of longitudinal wave velocity (%) |
|---|---|---|---|---|---|---|
| | | | | Before immersion | After immersion | |
| JZ-1 | 2,704.4 | 0.383 | 0.424 | 4,761.9 | 4,210.5 | 11.6 |
| JZ-2 | 2,685.8 | 0.415 | 0.632 | 4,522.3 | 3,860.2 | 14.6 |
| JZ-3 | 2,671.5 | 0.470 | 0.728 | 4,210.5 | 3,508.8 | 16.7 |
| JH-1 | 2,691.5 | 0.186 | 0.062 | 4,601.7 | 4,426.8 | 3.8 |
| JH-2 | 2,673.1 | 0.234 | 0.090 | 4,296.8 | 4,101.5 | 4.5 |
| JH-3 | 2,701.6 | 0.172 | 0.055 | 4,698.2 | 4,536.3 | 3.4 |

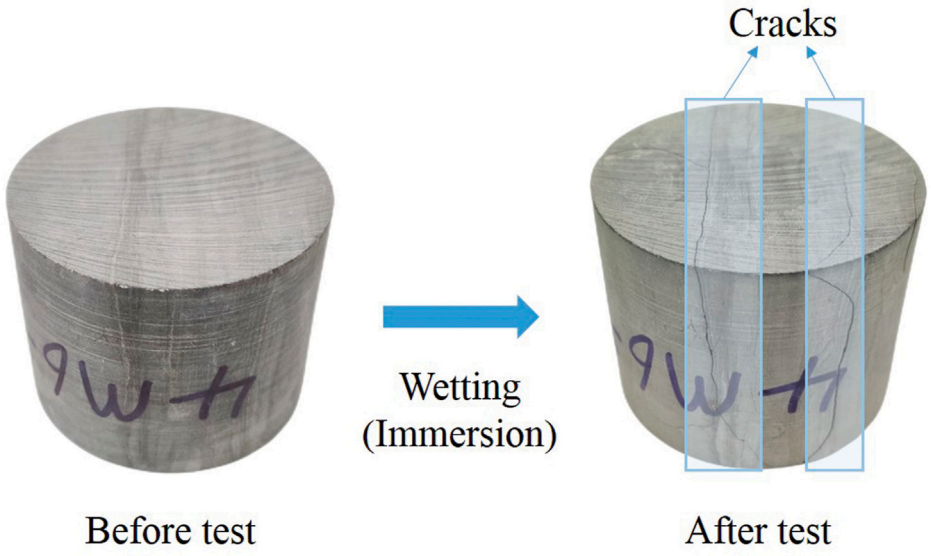


FIGURE 5
Comparison of samples with vertical interlayer before and after wetting and deterioration.

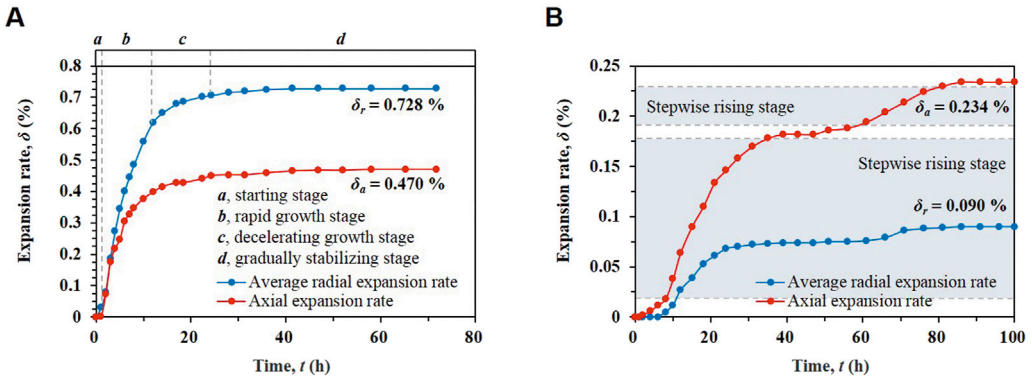


FIGURE 6
Three-way expansion rate time history curve **(A)** sample with vertical interlayer **(B)** sample with horizontal interlayer.

the next rapid growth stage until gradually stable. The final average radial expansion rate of the sample was 0.090%, and the axial expansion rate was 0.234%.

It could be seen from the three-way expansion rate test results that for the sample with vertical interlayer, the axial expansion rate of rock generally lagged behind the radial expansion rate. The rock first cracked along the interlayer plane to form a main crack, and the interlayer direction of the sample was not completely vertical under natural conditions, so the axial volume expansion component would be generated during the cracking along the interlayer direction, this was also the reason why the final axial expansion rate did not have a high multiple gap with the radial expansion rate. However, for the sample with horizontal interlayer, due to its own gravity, the interlayer gap was relatively tight, and it was difficult for water to enter into the rock and react with anhydrite to cause expansion cracking. Its expansion speed was slower than that of the sample with vertical interlayer, and it developed in a gradual and progressive manner.

The test results of rock longitudinal wave velocity showed that the rock longitudinal wave velocity decreased to varying degrees after the samples were immersed in water and deteriorated. The longitudinal wave velocity of the sample with vertical interlayer decreased more than that of the sample with horizontal interlayer. The longitudinal wave velocity of samples with vertical interlayer JZ-1, JZ-2 and JZ-3 decreased by 11.6%, 14.6% and 16.7% respectively, while that of samples with horizontal interlayer JH-1, JH-2 and JH-3 decreased by 3.8%, 4.5% and 3.4% respectively. The speed of longitudinal wave propagation was positively related to the compactness of rock. The denser the rock was, the faster the longitudinal wave propagation in the rock was. After the sample was deteriorated by immersion, its internal cracks developed. When the ultrasonic wave propagated along the test direction, it would diffract because it passed through discontinuities such as pores and cracks in the rock. If the number of times of diffraction was more, the actual distance in the acoustic wave propagation process was longer, which led to the lower transmission speed of the acoustic wave in the rock.

# 4 Analysis of rock compression evolution process

## 4.1 Sample selection

In order to study the influence of wetting deterioration of layered rock and interlayer effect on rock cracking and expansion, we continued to take the above JZ-1, JZ-2 and JZ-3 samples after air drying and record them as Group A, JH-1, JH-2 and JH-3 samples after air drying and record them as Group B, and took three undisturbed samples containing vertical and horizontal interlayer and record them as Group C and Group D respectively for rock uniaxial compression test.

## 4.2 Test equipment and process

The test was carried out on the RMT-150C multi-function rock testing machine in the Institute of Rock and Soil Mechanics, Chinese Academy of Sciences. This testing machine can complete a variety of rock mechanics tests such as uniaxial compression, uniaxial indirect tension, triaxial compression and shear, and its maximum vertical output is 1,000 kN. Before the test, a layer of Vaseline should be evenly coated on the upper and lower end faces of the sample to reduce the end effect of rock under uniaxial compression. The loading mode of the testing machine was set as axial displacement control, and the loading rate was set as 0.002 mm/s. During the test, radial and axial strain displacement sensors were used to monitor the deformation of rock (Figure 7).

## 4.3 Crack volume strain characteristics

Martin and Chandler (1994) put forward the calculation method of crack volume strain in the process of uniaxial compression of rock, and believed that the volume strain of rock was composed of elastic volume strain and crack volume strain. The calculation of crack volume strain could be obtained by subtracting the elastic volume strain from the total volume strain. According to crack volume strain curve, total volume strain curve and stress-strain curve, the whole compression process of rock was divided into five stages, crack closure stage, elastic stage, stable crack expansion stage, unstable crack expansion stage and post peak deformation stage.

The volume strain of rock $\varepsilon_v$ could be calculated from the axial strain $\varepsilon_1$ and radial strain $\varepsilon_3$ measured by the strain displacement sensor according to Eq. (1).

$$\varepsilon_v = \varepsilon_1 + 2\varepsilon_3 \tag{1}$$

The rock elastic modulus $E$ and Poisson's ratio $\nu$ could be calculated from the rock stress-strain curve. Since the three principal stresses $\sigma_1$, $\sigma_2$, $\sigma_3$, $\sigma_2 = \sigma_3 = 0$, the elastic volumetric strain $\varepsilon_v^e$ of the rock was

$$\varepsilon_v^e = \frac{1-2\nu}{E}\sigma_1 \tag{2}$$

According to the crack strain model, the crack volume strain $\varepsilon_v^c$ was

$$\varepsilon_v^c = \varepsilon_v - \varepsilon_v^e \tag{3}$$

The typical samples of each group were taken respectively. The crack volume strain curve and total volume strain curve were shown in Figure 8. The characteristic parameters of the test process were shown in Table 2.

The uniaxial compressive strength of each sample decreased after immersion, while the deformation of the sample increased along the radial direction, and the plastic characteristics were

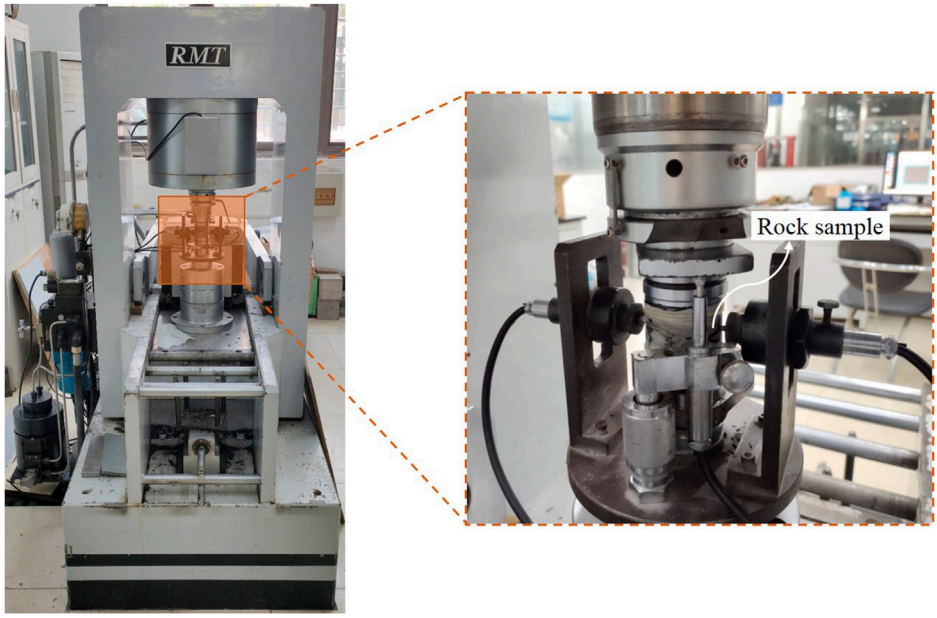


FIGURE 7
Uniaxial compression test of rock.

enhanced. The average uniaxial compressive strength of the sample with horizontal interlayer before and after immersion decreased from 170.22 MPa to 154.3 MPa, with a decrease rate of 9.35%. The average uniaxial compressive strength of the sample with vertical interlayer before and after immersion decreased from 104.45 MPa to 86.44 MPa, with a decrease rate of 17.24%. The average radial peak strain of the sample with horizontal interlayer before and after immersion increased from 0.10% to 0.12%, with an increase ratio of 20%. The average radial peak strain of the sample with vertical interlayer before and after immersion increased from 0.14% to 0.17%, with an increase ratio of 21.43%. It could be seen that the wetting effect had obvious deterioration effect on intercalated dolomite, which made the mechanical properties of rock decline, the deformation increased during the test, and the bearing failure changed to plastic failure. The direction of interlayer also had an important influence on the compressive strength and peak strain of rock. The compressive strength of the sample with vertical interlayer was obviously smaller than that of the sample with horizontal interlayer, and the peak radial strain was larger. Therefore, after wetting and deterioration, the rock had the weakest compressive property and the most obvious cracking expansion capacity under the force along the interlayer.

The whole loading process of rock could be divided into five stages by the four stress thresholds of crack closure stress $\sigma_{cc}$, crack initiation stress $\sigma_{ci}$, expansion stress $\sigma_{cd}$ and peak stress $\sigma_f$: crack closure stage, elastic deformation stage, stable crack growth stage, unstable crack growth stage and post failure peak stage.

When the rock was initially compressed, the internal primary cracks and pores were compacted, and the crack volume decreased until the crack closure stress was reached. The calculated crack volume strain was zero. In this crack closure stage (stage I), the axial and radial stress-strain curves of rock were generally concave, that was, the relationship between stress and strain was nonlinear. With the continuous loading, the rock entered the elastic deformation stage (stage II), and the calculated crack volume strain basically maintained at the zero growth level; The axial and radial strains increased linearly with the increase of stress, and the total volume strain also increased in a linear manner, and the rock continued to be compressed. When the rock stress exceeded the crack initiation stress, the cracks in the rock began to continue to develop, thus entering the stable crack growth stage (stage III), at which time the calculated crack volume strain increased from zero; The axial and radial strains and the total volume strain began to break away from the linear deformation. As the rock compression reached the limit and began to expand, the rock began to enter the unstable crack growth stage (stage IV). The stress corresponding to the reverse bending point of the volume strain curve was the expansion stress. Many researchers generally believed that the expansion stress was an indicator to determine the long-term strength of the rock (Bai et al., 2019; Bai et al., 2022; Zhou Y. Q. et al., 2022).

The ratio of crack initiation stress to peak stress $\sigma_{ci}/\sigma_f$ was taken as the crack initiation level; The ratio of expansion stress to peak stress $\sigma_{cd}/\sigma_f$ was taken as the expansion level. The calculation results of each sample are shown in Table 2.

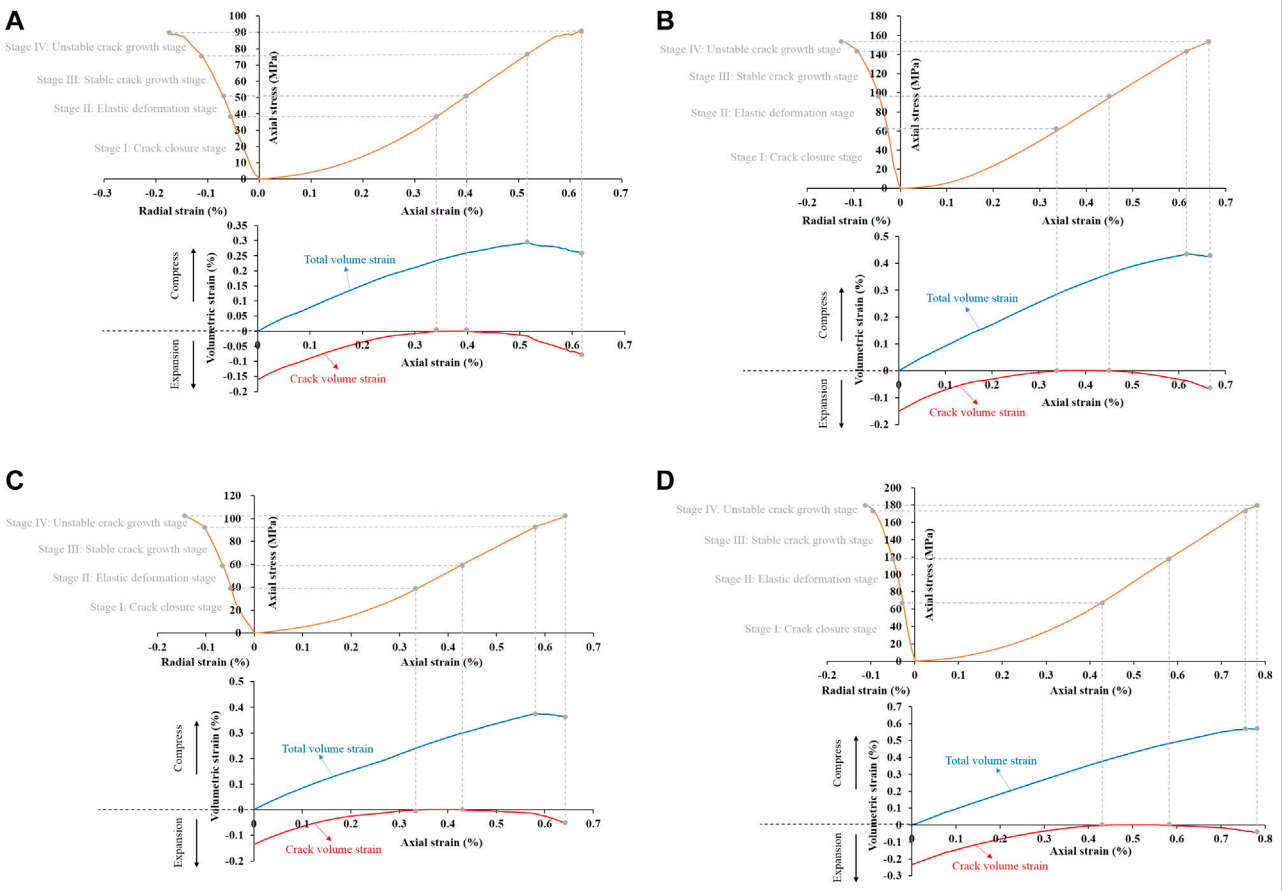


FIGURE 8
Stress-strain, total volume strain and crack volume strain curve of sample in uniaxial compression process **(A)** Sample with vertical interlayer after immersion **(B)** Sample with horizontal interlayer after immersion **(C)** Undisturbed sample with vertical interlayer **(D)** Undisturbed sample with horizontal interlayer.

The crack initiation level reflected the degree of defects existing in the rock, such as the difference in the internal structure of the rock and the dispersion of microcracks, grain boundaries and lattice defects (Wang et al., 2014; Hou et al., 2019). The larger the value was, the less fully developed the micro cracks in the rock were, and the more homogeneous the structure was. In addition, the crack initiation level and expansion level also reflected the relative difficulty of the initiation and development of different rock cracks in their stress deterioration stage to a certain extent.

After water immersion and air drying, the crack initiation level and expansion level of the samples with vertical interlayer (Group A) were the minimum, 0.560 and 0.837 respectively; The undisturbed samples with horizontal interlayer (Group D) were the largest, 0.616 and 0.978 respectively. However, the two values of the original sample containing vertical interlayer (Group C) and the sample containing horizontal interlayer after wetting and air drying (Group B) were between the two. The effect of sample wetting deterioration and the direction of interlayer had significant effects on the crack initiation level and expansion level of the sample under uniaxial compression. After wetting and deterioration, the external force required for rock cracking and expansion due to the force along the interlayer direction was the minimum, and the plastic stage of the sample was relatively long, with low brittleness, showing large plastic deformation, fully showing the effect of cracking and expansion. For the sample without wetting and deterioration, when the rock entered the plastic state during loading, it reached the peak stress in a short time, showing obvious brittle failure, relatively weak crack expansion effect, and the sample with the interlayer direction perpendicular to the stress direction showed more obvious brittle characteristics than the sample with the interlayer direction parallel to the stress direction.

TABLE 2 Characteristic parameters of compression process.

| Sample no. | | $\sigma_{ci}$ (MPa) | $\sigma_{cd}$ (MPa) | $\sigma_f$ (MPa) | Axial peak strain (%) | Radial peak strain (%) | Crack initiation level | Expansion level | Average crack initiation level | Average expansion level |
|---|---|---|---|---|---|---|---|---|---|---|
| Group A | JZ-1 | 51.327 | 76.404 | 90.481 | 0.616 | 0.178 | 0.567 | 0.844 | 0.560 | 0.837 |
| | JZ-2 | 46.685 | 69.402 | 83.516 | 0.585 | 0.163 | 0.559 | 0.831 | | |
| | JZ-3 | 47.185 | 71.332 | 85.325 | 0.591 | 0.169 | 0.553 | 0.836 | | |
| Group B | JH-1 | 90.604 | 144.018 | 152.676 | 0.665 | 0.120 | 0.593 | 0.943 | 0.597 | 0.946 |
| | JH-2 | 92.155 | 146.182 | 154.363 | 0.671 | 0.122 | 0.597 | 0.947 | | |
| | JH-3 | 93.536 | 147.942 | 155.893 | 0.675 | 0.122 | 0.600 | 0.949 | | |
| Group C | Z-1 | 67.278 | 104.089 | 113.263 | 0.643 | 0.141 | 0.594 | 0.919 | 0.589 | 0.914 |
| | Z-2 | 59.771 | 92.631 | 101.390 | 0.641 | 0.139 | 0.590 | 0.914 | | |
| | Z-3 | 57.538 | 89.613 | 98.693 | 0.637 | 0.136 | 0.583 | 0.908 | | |
| Group D | H-1 | 110.018 | 175.696 | 178.314 | 0.777 | 0.106 | 0.617 | 0.985 | 0.616 | 0.978 |
| | H-2 | 108.250 | 170.830 | 174.316 | 0.747 | 0.110 | 0.621 | 0.980 | | |
| | H-3 | 96.556 | 153.131 | 158.030 | 0.690 | 0.089 | 0.611 | 0.969 | | |

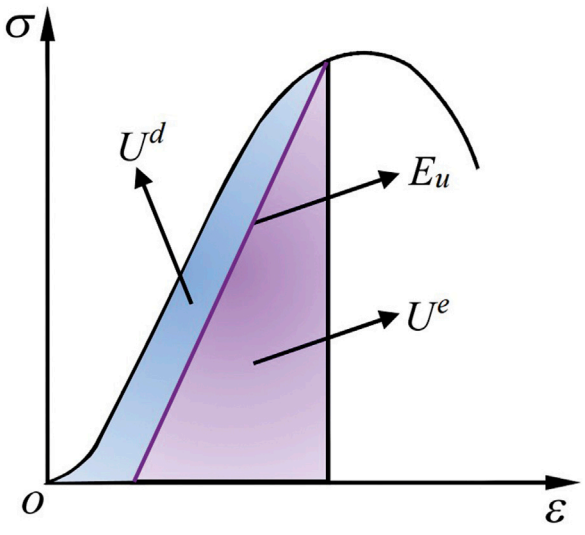


FIGURE 9
Schematic diagram of energy relationship in unit volume rock.

## 4.4 Energy dissipation characteristics

The process of rock uniaxial compression was analyzed from the aspect of energy dissipation. The energy change of rock in the process of uniaxial compression included the input of strain energy generated by external force work, the storage of releasable elastic strain energy and the irreversible loss of dissipated energy (Xie et al., 2005). Assuming that in a closed system, rocks were deformed by external forces, it could be concluded from the first law of thermodynamics that:

$$U = U^e + U^d \tag{4}$$

Where, $U$ is the total strain energy per unit volume of rock generated by external force work, $U^e$ is the elastic strain energy per unit volume of rock that can be released, and $U^d$ is the dissipated energy per unit volume of rock.

Figure 9 shows the relationship among $U$, $U^e$ and $U^d$ in the stress-strain curve of rock under uniaxial compression. The total strain energy per unit volume of rock generated by external work $U$ was the area enclosed by the stress-strain curve and the coordinate axis, which could be obtained by integrating the corresponding stress-strain curve; The released elastic strain energy per unit volume of rock $U^e$ was the area of the shaded part in Figure 9, that was, the area enclosed by the unloading elastic modulus $E_u$ and the coordinate axis. According to the test results (Xie et al., 2005; You et al., 2001; Liang et al., 2015), the unloading elastic modulus $E_u$ could be approximately taken as the initial elastic modulus $E_0$; The dissipated energy per unit volume of rock $U^e$ was the area enclosed by the stress-strain curve and unloading elastic modulus $E_u$. The dissipated energy was mainly accompanied by the internal damage and plastic deformation of rock.

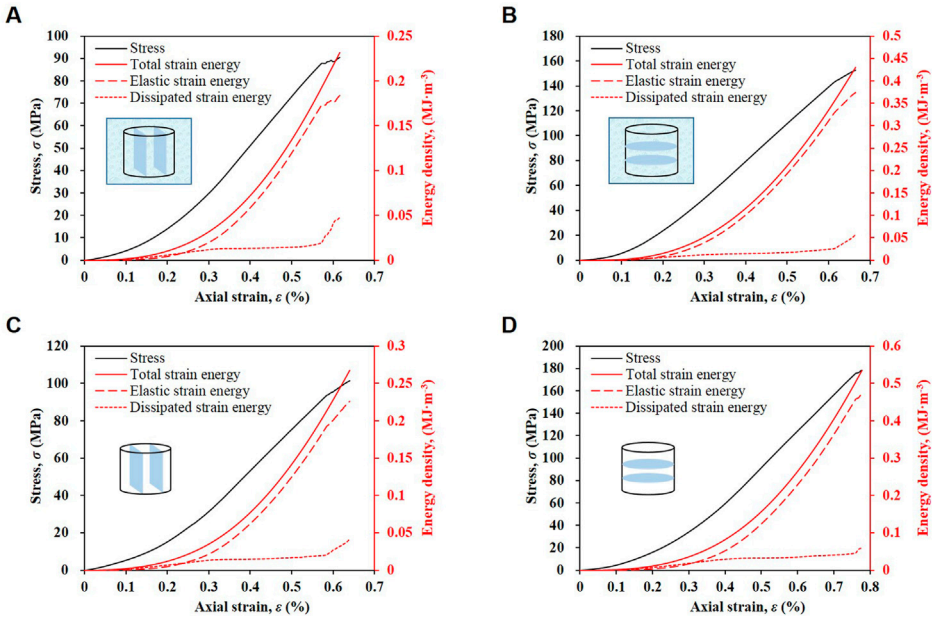


FIGURE 10
Relation curves between strain energy density and axial strain of rock samples under different initial conditions **(A)** Sample with vertical interlayer after immersion **(B)** Sample with horizontal interlayer after immersion **(C)** Undisturbed sample with vertical interlayer **(D)** Undisturbed sample with horizontal interlayer.

According to the above analysis, the total strain energy per unit volume of rock generated by external force work $U$, the released elastic strain energy per unit volume of rock $U^e$ and the dissipated energy per unit volume of rock $U^d$ could be calculated by Equations (5–7) respectively:

$$U = \frac{1}{2}\sum_{i=1}^{n}\left(\sigma_{h(i)} + \sigma_{h(i-1)}\right)\left(\varepsilon_{h(i)} - \varepsilon_{h(i-1)}\right) \tag{5}$$

$$U^e = \frac{\sigma_{h(i)}^2}{2E_0} \tag{6}$$

$$U^d = U - U^e = \frac{1}{2}\sum_{i=1}^{n}\left(\sigma_{h(i)} + \sigma_{h(i-1)}\right)\left(\varepsilon_{h(i)} - \varepsilon_{h(i-1)}\right) - U^e = \frac{\sigma_{h(i)}^2}{2E_0} \tag{7}$$

Where, $\sigma_{h(i)}$ and $\varepsilon_{h(i)}$ are the stress and axial strain values at the point $h(i)$ on the stress-strain curve respectively; $\sigma_{h(i\text{-}1)}$ and $\varepsilon_{h(i\text{-}1)}$ are the stress and axial strain values at the point $h$ ($i$-1) on the stress-strain curve respectively.

It can be seen from Figure 10 that the total strain energy of each sample increased with a concave tendency. The elastic strain energy first showed a concave growth, and then became irregular growth or small amplitude oscillation after reaching a certain value. The dissipative strain energy first showed a convex growth, that was, the initial growth was fast, then slowed down, and then started to increase significantly at a certain value. The variation characteristics of rock energy curve could reflect the crack development and energy evolution during rock compression. In the initial compaction stage, the primary cracks closed and consumed more energy, and the dissipated strain energy in this stage was roughly equal to the elastic strain energy. When the sample entered the elastic deformation stage, at this time, the crack volume strain was almost zero, and there was basically no damage in the rock. Therefore, almost all the energy input due to the work done by the external force was converted into elastic strain energy and stored in the rock. The elastic strain energy curve was basically parallel to the total strain energy curve, while the curve of the dissipative strain energy was approximately horizontal due to no growth. In the stable crack growth stage, the dissipative strain energy started to increase slightly, which indicated that the sample began to regenerate damage cracks and produced irreversible plastic deformation. After the sample entered the unstable crack growth stage, its internal cracks were rapidly generated, developed and connected. The total volume strain changed from compression to expansion, and the dissipated strain energy increased significantly. Although the elastic strain energy was still accumulating inside the rock, its growth rate slowed down until it reached a limit, and the elastic strain energy was rapidly released to finally destroyed the rock as a whole (Xie et al., 2005).

Table 3 shows the results of energy characteristic values obtained from rock uniaxial compression tests under different initial conditions. The ratio of the dissipative strain energy density and the elastic strain energy density to the total strain energy density was taken as the dissipative energy conversion rate and the elastic energy conversion rate, respectively. The energy conversion rate had an

TABLE 3 Characteristic parameters of compression energy.

| Sample no. | | Total strain energy (kJ/m$^3$) | Elastic strain energy (kJ/m$^3$) | Dissipated strain energy (kJ/m$^3$) | Dissipated energy conversion rate (%) | Elastic energy conversion rate (%) | Average energy dissipation conversion rate (%) | Average elastic energy conversion rate (%) |
|---|---|---|---|---|---|---|---|---|
| Group A | JZ-1 | 231.42 | 183.73 | 47.69 | 20.61 | 79.39 | 23.58 | 76.42 |
| | JZ-2 | 210.03 | 156.77 | 53.26 | 25.36 | 74.64 | | |
| | JZ-3 | 215.56 | 162.17 | 53.39 | 24.77 | 75.23 | | |
| Group B | JH-1 | 430.87 | 374.01 | 56.86 | 13.20 | 86.80 | 12.80 | 87.20 |
| | JH-2 | 437.96 | 381.86 | 56.10 | 12.81 | 87.19 | | |
| | JH-3 | 442.12 | 387.39 | 54.73 | 12.38 | 87.62 | | |
| Group C | Z-1 | 299.56 | 257.23 | 42.33 | 14.13 | 85.87 | 15.57 | 84.43 |
| | Z-2 | 267.38 | 226.28 | 41.10 | 15.37 | 84.63 | | |
| | Z-3 | 258.63 | 214.12 | 44.51 | 17.21 | 82.79 | | |
| Group D | H-1 | 535.85 | 472.93 | 62.93 | 11.74 | 88.26 | 11.87 | 88.13 |
| | H-2 | 523.67 | 461.56 | 62.11 | 11.86 | 88.14 | | |
| | H-3 | 455.86 | 401.11 | 54.75 | 12.01 | 87.99 | | |

important influence on the characteristics of the rock compression evolution process (Zhang et al., 2019). The results show that the undisturbed rock with horizontal interlayer without water immersion needed the most external input energy in the process of vertical compression failure, and was the most difficult to be damaged. In the process of compression, the external force work was mainly converted into elastic strain energy and stored in the rock. When the peak stress was reached, the average elastic energy conversion rate was 88.13%. However, the proportion of energy dissipated by plastic deformation such as crack generation and development and friction between cracks was very small, which indicated that the whole compression process showed obvious brittleness, and the cracking expansion was concentrated at the moment of rock failure. However, after immersion, the threshold value of elastic strain energy density required for failure of rock with horizontal interlayer decreased, and the conversion rate of dissipated energy and the plasticity increased during compression. The average value of external input energy required for failure of undisturbed samples with vertical interlayer without water immersion was only 54.48% of that of undisturbed samples with horizontal interlayer under the same conditions, which fully indicated that the angle between the direction of rock stress and the direction of interlayer determined the degree of rock failure. For the sample with vertical interlayer, the average value of external input energy required for failure after immersion had decreased by 20.42%, and the average value of energy conversion rate of dissipation had also significantly increased from 15.57% to 23.58%, which indicated that the rock had undergone relatively sufficient wetting and deterioration during immersion, resulting in the continuous development and expansion of cracks and the enhancement of plastic characteristics of the rock during compression under force.

## 5 Conclusion

1) The rock sample had obvious interlayer structure and its mineral composition contained anhydrite, an expansive material and hydrophilic clay mineral, which made the sample had the deterioration potential of cracking and expansion after immersion.
2) The three-way expansion rate test of rock showed that the sample with vertical interlayer showed the deterioration characteristics of micro expansion and cracking along the direction of interlayer after wetting, and its expansion process included four stages: starting stage, rapid growth stage, decelerating growth stage and gradually stabilizing stage. However, the axial and radial expansion rates of samples with horizontal interlayer were obviously lower than those with vertical interlayer after immersion, and the expansion process presented a hierarchical and progressive development.
3) Before and after immersion, the longitudinal wave velocity of the ultrasonic wave passing through the sample decreased, but the decrease amplitude of the sample with vertical interlayer was obviously larger than that of the sample with horizontal interlayer, and the average decrease rate was 14.3% and 3.9% respectively. It reflected that the development of internal cracks occurred in all samples after immersion, and the wetting deterioration effect of samples with vertical interlayer was more significant than that of samples with horizontal interlayer.
4) The crack volume strain method was used to analyze the evolution process of rock under uniaxial compression. The test results showed that the uniaxial compressive strength, crack initiation level, and expansion level of the sample had

decreased after wetting and deterioration, while the radial peak strain of the sample had increased, and the change amplitude of the sample with vertical interlayer was greater than that of the sample with horizontal interlayer before and after wetting, and the cracking expansion and plasticity were more obvious.

5) In terms of energy conversion in uniaxial compression process, the threshold value of the elastic strain energy density required for the sample to reach failure decreased after wetting, and the threshold value of the sample with vertical interlayer was smaller than that of the sample with horizontal interlayer before and after immersion. The dissipative energy conversion rate to reflect the plastic deformation such as crack generation, expansion and friction between cracks of the undisturbed sample with vertical interlayer was significantly higher than that of the undisturbed sample with horizontal interlayer, and the growth rate was greater after wetting. The average dissipative energy conversion rate of the sample with vertical interlayer increased from 15.57% to 23.58%, and the average dissipative energy conversion rate of the sample with horizontal interlayer increased from 11.87% to 12.80%.

## Data availability statement

The original contributions presented in the study are included in the article/supplementary material, further inquiries can be directed to the corresponding author.

## Author contributions

ZD: Writing—review and editing, Supervision, Validation, Funding acquisition. YW: Data curation, Methodology, Writing—original draft. ZZ: Data curation, Investigation. JL: Validation. FY: Methodology, Investigation. SC: Project administration, Supervision.

## Funding

The work reported in this paper was financially supported by the National Natural Science Foundation of China (No. 42172308), the Youth Innovation Promotion Association CAS (No. 2022331) and the Key Research and Development Program of Hubei Province (No. 2022BAA036).

## Acknowledgments

We would like to acknowledge the reviewers and the editors for their comments and suggestions.

## Conflict of interest

The authors declare that the research was conducted in the absence of any commercial or financial relationships that could be construed as a potential conflict of interest.

## Publisher's note



## References

Anderson, D. L., Minster, B., and Cole, D. (1974). The effect of oriented cracks on seismic velocities. *J. Geophys. Res.* 79 (26), 4011–4015. doi:10.1029/JB079i026p04011

Bai, B., Wang, Y., Rao, D., and Bai, F. (2022). The effective thermal conductivity of unsaturated porous media deduced by pore-scale SPH simulation. *Front. Earth Sci. (Lausanne).* 10, 943853. doi:10.3389/feart.2022.943853

Bai, B., Yang, G., Li, T., and Yang, G. (2019). A thermodynamic constitutive model with temperature effect based on particle rearrangement for geomaterials. *Mech. Mater.* 139, 103180. doi:10.1016/j.mechmat.2019.103180

Bai, B., Zhou, R., Cai, G., Hu, W., and Yang, G. (2021). Coupled thermo-hydro-mechanical mechanism in view of the soil particle rearrangement of granular thermodynamics. *Comput. Geotechnics* 137 (8), 104272. doi:10.1016/j.compgeo.2021.104272

Cai, G., Cheng, Y., Zhong, C., Jia, J., Zhao, D., and Feng, W. (2021). Experimental on softening effect of phyllite in saturated water. *Sci. Technol. Eng.* 21 (8), 3032–3038.

Chai, Z., Zhang, Y., and Zhang, X. (2015). Experimental investigations on correlation with slake durability and mineral composition of mudstone. *J. China Coal Soc.* 40 (5), 1188–1193. doi:10.13225/j.cnki.jccs.2014.0897

Diao, X., Yang, S., and Mao, X. (2017). Experimental study on water absorption and expansion characteristics of mudstone under conditions of different temperature and humidity. *J. East China Jiaot. Univ.* 34 (3), 14–18. doi:10.16749/j.cnki.jecjtu.2017.03.003

Du, W., Sheng, Q., Fu, X., Chen, J., and Zhou, Y. (2022). A TPDP-MPM-based approach to understanding the evolution mechanism of landslide-induced disaster chain. *J. Rock Mech. Geotechnical Eng.* 14 (4), 1200–1209. doi:10.1016/j.jrmge.2022.03.004

Feng, Z., Xu, Q., Luo, X., Huang, R., Liao, X., and Tang, Q. (2022). Microstructure, deformation characteristics and energy analysis of mudstone under water absorption process. *Energies* 15 (20), 7511. doi:10.3390/en15207511

Fu, X., D, H., Sheng, Q., Zhang, Z., Yin, D., and Chen, F. (2022). Fractal analysis of particle distribution and scale effect in a soil-rock mixture. *Fractal Fract.* 6 (2), 120. doi:10.3390/fractalfract6020120

He, M., Wei, L., Jia, Y., Huang, A., Wang, J., and Huang, X. (2019). Experimental study on expansive mechanical characteristics of red-bed soft rock. *Water Resour. Hydropower Eng.* 50 (4), 171–178. doi:10.13928/j.cnki.wrahe.2019.04.024

He, Q., Sun, L., Song, J., Ding, B., and Wang, Z. (2022). Association between sleep duration and hypertension among adults in southwest China. *Glob. Heart* 45 (5), 10–1217. doi:10.5334/gh.1100

Hou, Z., Wang, Y., Liu, D., and Li, C. (2019). Investigation of the anisotropic mechanical behaviors and energy evolution during uniaxial deformation of interbedded marble. *J. Min. Saf. Eng.* 36 (4), 794–804. doi:10.13545/j.cnki.jmse.2019.04.019

Hua, W., Li, J., Dong, S., and Pan, X. (2019). Experimental study on mixed mode fracture behavior of sandstone under water-rock interactions. *Processes* 7 (2), 70. doi:10.3390/pr7020070

Jia, H., Wang, E., Song, D., Wang, X., and Ali, M. (2019). Precursory changes in wave velocity for coal and rock samples under cyclic loading. *Results Phys.* 12, 432–434. doi:10.1016/j.rinp.2018.11.096

Jiang, J., Hou, Z., Hou, K., Lu, Y., Sun, H., and Niu, X. (2022). The damage constitutive model of sandstone under water-rock coupling. *Geofluids* 2022, 1–12. doi:10.1155/2022/1731254

Jiang, J., Xiang, W., Rohn, J., Zeng, W., and Schleier, M. (2015). Research on water-rock (soil) interaction by dynamic tracing method for Huangtupo landslide, Three Gorges Reservoir, PR China. *Environ. Earth Sci.* 74 (1), 557–571. doi:10.1007/s12665-015-4068-5

King, M. S., Chaudhry, N. A., and Shakeel, A. (1995). Experimental ultrasonic velocities and permeability for sandstones with aligned cracks. *Int. J. Rock Mech. Min. Sci. Geomechanics Abstr.* 32 (2), 155–163. doi:10.1016/0148-9062(94)00033-Y

Li, S., Huang, Z., Liang, Q., Liu, J., Luo, S., and Zhou, W. (2022). Evolution mechanism of mesocrack and macrocrack propagation in carbonaceous mudstone under the action of dry-wet cycles. *Geofluids* 2022, 1–8. doi:10.1155/2022/6768370

Liang, C., Wu, S., Li, X., and Xin, P. (2015). Effects of strain rate on fracture characteristics and mesoscopic failure mechanisms of granite. *Int. J. Rock Mech. Min. Sci. (1997).* 76, 146–154. doi:10.1016/j.ijrmms.2015.03.010

Ma, L. (2015). *Research on low clay mineral mudstone expansion mechanism and influence for high-speed railway subgrade*. dissertation (Lanzhou: Lanzhou Jiaotong University).

Martin, C. D., and Chandler, N. A. (1994). The progressive fracture of Lac du Bonnet granite. *Int. J. Rock Mech. Min. Sci. Geomechanics Abstr.* 31 (6), 643–659. doi:10.1016/0148-9062(94)90005-1

Song, Y., Chen, J., Zhang, L., Ren, J., Che, Y., and Yang, H. (2021). Damage and degradation characteristics of loaded sandstone under drying-wetting cycles. *J. Yangtze River Sci. Res. Inst.* 38 (9), 133–140. doi:10.11988/ckyyb.20200679

Tang, Y., Hao, T., Li, F., Zhao, L., and Liu, J. (2022). Energy evolution and infrared radiation characterization of coal rocks considering strain rate effect. *Chin. J. Rock Mech. Eng.* 41 (6), 1126–1135. doi:10.13722/j.cnki.jrme.2021.0952

Wang, Y., Li, X., Wu, Y., Ben, Y., Li, S., He, J., et al. (2014). Research on relationship between crack initiation stress level and brittleness indices for brittle rocks. *Chin. J. Rock Mech. Eng.* 33 (2), 264–275. doi:10.13722/j.cnki.jrme.2014.02.003

Xie, H., Ju, Y., and Li, L. (2005). Criteria for strength and structual failure of rocks based on energy dissipation and energy release principles. *Chin. J. Rock Mech. Eng.* 24 (17), 3003–3010.

Yang, S. (2017). *Study on Hygroscopic properties of expansive rock under high temperature and high humidity environment*. master's thesis (Nanchang: East China Jiaotong University).

You, M., Su, C., and Xu, T. (2001). Loading or unloading process in axial direction and Young's modulus of rock specimen. *Chin. J. Geotechnical Eng.* 23 (5), 588–592.

Zeng, L., Liu, J., Gao, Q., and Bian, H. (2019). Evolution characteristics of the cracks in the completely disintegrated carbonaceous mudstone subjected to cyclic wetting and drying. *Adv. Civ. Eng.* 2019, 1–10. doi:10.1155/2019/1279695

Zhang, J., Xi, X., Guo, Q., and Wu, X. (2021). Meso multi-phase particle flow simulation of granite failure with preexisting crack. *J. Huazhong Univ. Sci. Tech. Nat. Sci. Ed.* 49 (4), 79–85. doi:10.13245/j.hust.210413

Zhang, X., Lü, G., Zhang, Q., Liu, Q., Li, W., and Xu, J. (2020). Uniaxial compression test for three stress thresholds of siliceous siltstone. *J. Eng. Geol.* 28 (3), 441–449. doi:10.13544/j.cnki.jeg.2019-085

Zhang, Z., Xie, H., Zhang, R., Zhang, Z., Gao, M., Jia, Z., et al. (2019). Deformation damage and energy evolution characteristics of coal at different depths. *Rock Mech. Rock Eng.* 52 (5), 1491–1503. doi:10.1007/s00603-018-1555-5

Zhao, Z., Liu, H., Lyu, X., Wang, L., Tian, Z., and Sun, J. (2021). Experimental study on the damage and deterioration behaviour of deep soft rock under water-rock interaction. *Geofluids* 2021, 1–11. doi:10.1155/2021/8811110

Zhou, C., Deng, Y., Tan, X., Liu, Z., Shang, W., and Zhan, S. (2005). Experimental research on the softening of mechanical properties of saturated soft rocks and application. *Chin. J. Rock Mech. Eng.* 24 (1), 33–38.

Zhou, K., Dou, L., Gong, S., Chai, Y., Li, J., Ma, X., et al. (2022a). Mechanical behavior of sandstones under water-rock interactions. *Geomechanics Eng.* 29 (6), 627–643. doi:10.12989/gae.2022.29.6.627

Zhou, Y. Q., Sheng, Q., Li, N. N., and Fu, X. D. (2022b). The dynamic mechanical properties of a hard rock under true triaxial damage-controlled dynamic cyclic loading with different loading rates: A case study. *Rock Mech. Rock Eng.* 55 (4), 2471–2492. doi:10.1007/s00603-021-02756-w